THE JOURNAL OF PHYSICAL CHEMISTRY B
A JOURNAL OF THE AMERICAN CHEMICAL SOCIETY

pubs.acs.org/JPCB

Article

Dynamics of Hydrogen Bonds between Water and Intrinsically Disordered and Structured Regions of Proteins

Korey M. Reid, Humanath Poudel, and David M. Leitner*

Cite This: *J. Phys. Chem. B* 2023, 127, 7839−7847

Read Online

ACCESS | Metrics & More | Article Recommendations | Supporting Information

ABSTRACT: Recent studies indicate more restricted dynamics of water around intrinsically disordered proteins (IDPs) than structured proteins. We examine here the dynamics of hydrogen bonds between water molecules and two proteins, small ubiquitin-related modifier-1 (SUMO-1) and ubiquitin-conjugating enzyme E2I (UBC9), which we compare around intrinsically disordered regions (IDRs) and structured regions of these proteins. It has been recognized since some time that excluded volume effects, which influence access of water molecules to hydrogen-bonding sites, and the strength of hydrogen bonds between water and protein affect hydrogen bond lifetimes. While we find those two properties to mediate lifetimes of hydrogen bonds between water and protein residues in this study, we also find that the lifetimes are affected by the concentration of charged groups on other nearby residues. These factors are more important in determining the hydrogen bond lifetimes than whether a residue hydrogen bonding with water belongs to an IDR or to a structured region.

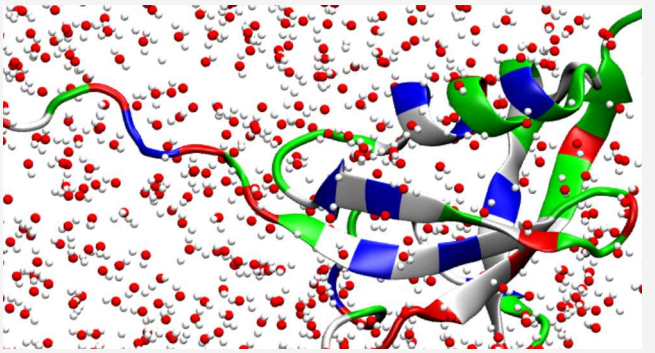

Downloaded via BOCHUM LIBRARIES on September 22, 2023 at 19:33:35 (UTC).
See https://pubs.acs.org/sharingguidelines for options on how to legitimately share published articles.

1. INTRODUCTION

Intrinsically disordered proteins (IDPs) and intrinsically disordered regions (IDRs) of otherwise structured proteins are ubiquitous and involved in many signaling and regulatory processes.[1−3] Interactions between proteins and water and the dynamics of water around proteins play key roles in protein function, including enzyme activity and allostery,[4,5] and while these properties have been extensively studied for structured proteins,[6−36] less is known for IDPs and proteins with IDRs. Some studies indicate more restricted dynamics of water around IDRs and IDPs compared to structured systems of similar size,[37−41] the origin of which appears to be due at least in large part to a greater presence of charged groups in disordered regions.[38] In a recent study of a family of disordered peptides results of molecular dynamics (MD) simulations and megahertz (MHz)-to-terahertz (THz) dielectric spectroscopic measurements indicated that the presence of charged groups underlies the more restrictive motion of water near the surface of the IDPs compared with two structured systems of similar size.[42] Moreover, it was found that near IDPs, the dynamics of water molecules around both charged and uncharged residues is more restricted than around corresponding groups of the structured systems, a result consistent with NMR measurements that found segments of three residues in sequence sharing collective behavior.[43] In this article, to clarify the possibility of collective effects near disordered regions on water dynamics, contributions of charged groups, and accessibility of water to protein residues, we examine hydrogen bond dynamics for water molecules around IDRs and structural elements of two proteins, small ubiquitin-related modifier-1 (SUMO-1) and ubiquitin-conjugating enzyme E2I (UBC9).

We recently studied the hydration layer and dynamics of water around three IDPs and two structured systems of similar size, all between 22 and 26 residues, to investigate differences in hydration water dynamics between IDPs and structured proteins and its origins.[42] The systems were either intrinsically disordered or structured. There was a clear distinction between dynamics of water near charged and neutral residues, with slower dynamics near charged groups, particularly anionic.[42] Moreover, there appeared to be a collective slowing down of water dynamics around the IDPs, where the dynamics of water around neutral residues was found to be more sluggish than around neutral and even some of the charged residues around the structured systems. The results of the MHz-to-THz measurements indicated overall more restricted water dynamics and more tightly bound water molecules around the IDP for which measurements were made than around the two structured systems. Rotational dynamics of water was probed in the experiments, while the MD simulations examined both

Received: May 10, 2023
Revised: August 21, 2023
Published: September 6, 2023

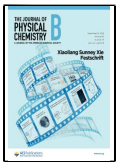

ACS Publications

© 2023 American Chemical Society

rotational and hydrogen bond dynamics, where the latter provided information about local dynamics involving charged and neutral residues of the IDPs and structured systems.

This study examines dynamics of hydrogen bonds between water and two proteins with both IDRs and structured regions, SUMO-1 and UBC9, illustrated in Figure 1. Small ubiquitin-related modifier protein-1 (SUMO-1) regulates a variety of cellular proteins by covalent linkage termed sumoylation. It regulates protein−protein interactions, protein−DNA interactions, and protein subcellular localization, and is important in the maintenance of cellular homeostasis as the cell responds to a variety of cellular stresses.[44,45] UBC9, a ubiquitin-conjugating enzyme, participates in the cycle of sumoylation of SUMO-1. There is evidence that liquid−liquid phase separation plays a key role in cellular sumoylation.[45] Both SUMO-1 and UBC9 contain numerous IDRs, regions that are generally implicated in liquid−liquid phase separation.[38,46] SUMO-1, with 101 amino acids of which 57 are in IDRs, is the smaller of the two. It contains 4 IDRs ranging in length from 6 to 21 amino acids. UBC9, with 158 amino acids of which 67 are in IDRs, contains 6 IDRs ranging in length from 3 to 31 amino acids. IDRs are associated with flexibility in interactions with a variety of systems important in regulation.[1] We note that liquid−liquid phase separation can give rise to a protein-rich phase with a high density of IDPs and a dilute phase,[38,46,47] and we are examining here properties of water around IDRs and structured regions of proteins in dilute solution.

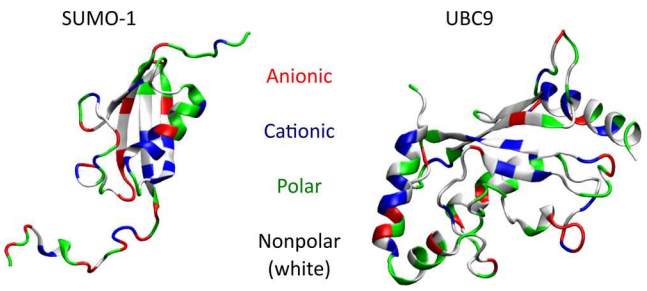

Figure 1. Structures of SUMO-1 and UBC9 colored by residue type: anionic, cationic, polar, and nonpolar.

In the earlier work,[42] it was seen that water dynamics, including the dynamics of hydrogen bonds between water and the protein, was more restricted near residues of IDPs, regardless of whether the residue is charged or neutral. The IDPs of that study had a higher concentration of charged groups than the structured proteins. The density of water molecules in the first hydration layer was larger, as was the number of water molecules tightly bound to the surface of the proteins, as revealed by analysis of the MHz-to-THz dielectric spectra. These results suggest that more tightly bound water molecules in contact with charged groups affect the dynamics of hydrogen bonds between water and nearby neutral residues.

We shall also see the importance of density of charged groups on the hydrogen bond dynamics of water and SUMO-1 and UBC9. The dynamics will be discussed in terms of models for hydrogen bond rearrangement, where the mobility of water molecules to serve as new hydrogen bond acceptors is taken into account.[48,49] Besides the concentration of charged groups, we will see that the solvent-accessible surface area of a particular residue relative to its largest value found in a large database[50] also plays a key role in the dynamics of hydrogen bonds between water and the protein. This so-called relative solvent-accessible surface area affects the extent to which water molecules can reach a water−protein hydrogen bond and form a new hydrogen bond. The combination of relative solvent-accessible surface area and density of charged groups will be seen to play a more decisive role in the dynamics of hydrogen bonds between water and SUMO-1 and UBC9 than whether the residue belongs to an IDR or a structured region.

The article is organized as follows: In Section 2, we summarize the computational methods used to examine the dynamics of water near SUMO-1 and UBC9. In Section 3, we present and discuss results of the computational study. Concluding remarks appear in Section 4.

2. METHODS

Human small ubiquitin-related modifier-1 (SUMO-1) and ubiquitin-conjugating enzyme E2I (UBC9) were simulated with the CHARMM 36m force field.[51,52] Simulations were performed with GROMACS 2019.6.[53,54] The initial configurations for SUMO-1 and UBC9 were taken from the Protein Data Bank (PDB)[55] entries 1A5R and 1A3S, respectively. Of note, simulations employing the Optimal Point Charge (OPC) water model with the Amber force field models ff99SB and ff14SB were tested for both systems. However, structural content of both SUMO-1 and UBC9 using these force fields proved unstable during long production simulations.

The systems were prepared in a truncated octahedral box with a minimum padding distance of 1.4 nm from either protein. The two systems were solvated with the TIP3P water model[56] optimized for use with CHARMM 36m[52] and NaCl was added to each system resulting in a 0.15 M salt concentration. The resulting systems contained 24,562 and 16,095 TIP3P water molecules for SUMO-1 and UBC9, respectively. A total of 74 Na^+ and 69 Cl^- ions are contained within the SUMO-1 system, while 47 Na^+ and 51 Cl^- are contained within the UBC9 system. Harmonic position restraints were applied in minimization and equilibration with a harmonic force constant of 1000 kJ mol^{-1} nm^{-2} where stated. Particle mesh Ewald[57] was employed for long-range electrostatics. Neighbor searching was performed by the Verlet[58] cutoff scheme where the Coulomb and van der Waals cutoff were both set to 1.2 nm, and force switching was applied for van der Waals interactions starting at 1.0 nm smoothly switching off at 1.2 nm. Temperature coupling was accomplished using the velocity rescale algorithm[59] with independent coupling of the protein and the remainder of molecules in the system. Time integration was performed every 2 fs, and periodic boundary conditions were applied in all three dimensions.

Both systems were minimized to 100.0 kJ mol^{-1} nm^{-1} with heavy-atom position restraints over 50,000 steps or until the cutoff was reached. Atom velocities were generated using a Maxwell distribution equating to 300 K and each system was simulated under a canonical ensemble with position-restrained heavy atoms at 300 K with a temperature coupling constant of 100 fs for 5 ns to relax the solvent. The systems were then simulated under an isobaric−isothermal (NPT) ensemble keeping the same temperature coupling constant and a pressure bath with a coupling constant of 2.0 ps for 1 ns with the Berendsen pressure bath to relax the density, followed by a 4 ns simulation with the Parrinello−Rahman pressure bath at 1 bar with heavy-atom position restraints applied. The

https://doi.org/10.1021/acs.jpcb.3c03102
J. Phys. Chem. B 2023, 127, 7839−7847

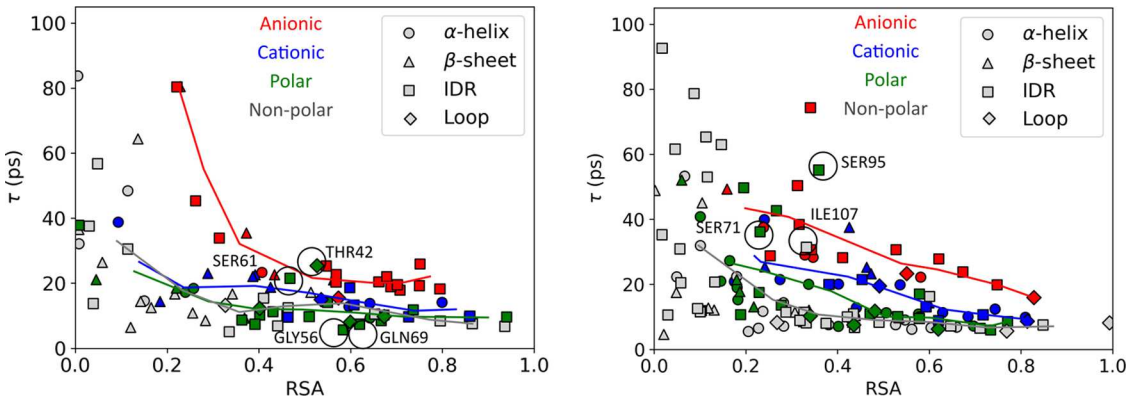

Figure 2. Hydrogen bond lifetime, τ, vs relative solvent-accessible surface area (RSA), defined by eq 2, plotted for residues of (left) SUMO-1 and (right) UBC9 with some of the outliers indicated. The residues and data points are colored by the residue side chain: (red) anionic, (blue) cationic, (green) polar, and (white) nonpolar.

final stage of equilibration was carried out without position restraints under the same NPT conditions for 100 ns.

For analysis of water dynamics, the production simulation was performed for a total of 55 ns under constant volume−isothermal (NVT) conditions, which was sufficient for convergence of properties studied here. The structural features of SUMO-1 and UBC9 remained unchanged over the course of this simulation time using the CHARMM 36m force field. The system was under the velocity rescale thermostat with a time constant of 1 ps at 300 K. Coordinates were saved every 250 fs for later analysis.

SUMO-1 and UBC9 differ in their disordered content. SUMO-1 is made up of 101 amino acids of which 57 are in IDRs. The 4 IDRs range in length from 6 to 21 amino acids. UBC9 contains 158 amino acids of which 67 are in IDRs. The 6 IDRs range in length from 3 to 31 amino acids. We investigate the dynamics of water near each residue, specifically within 3.5 Å. To assess the stickiness of the surface waters near each residue, the hydrogen bond time correlation function, $C(t)$, was investigated for hydrogen bonds between water molecules and the protein[13]

$$C(t) = \left\langle \frac{h(t_0)h(t_0 + t)}{h(t_0)^2} \right\rangle \tag{1}$$

This correlation function corresponds to the probability that a hydrogen bond between the protein and water exists at a time, t, after t_0, given that it was found at t_0, regardless of whether it broke in the meantime. In eq 1, $h(t)$ is 1 when there is a hydrogen bond and is otherwise 0. Hydrogen bonds are defined for D−H···A when D and A are within 3.5 Å and the DHA bond angle is greater than 150°. Lifetimes, τ, are taken to be the time where $C(t)$ is e^{-1} of $C(0)$, which is found via nonlinear least-squares fitting with the SciPy Python 3.6 library. This is the definition of hydrogen bond lifetime adopted in our previous study,[42] and we use the same for consistency. $C(t)$ is not a single exponential, and this time constant represents the fast decay. The full set of data for all $C(t)$ is available via a link provided in the Supporting Information.

Studies of the dynamics of hydrogen bonds between water molecules near proteins reveal the importance of charged groups on the dynamics, particularly anionic groups,[48] and the results presented here indicate this is also the case for protein−water hydrogen bonds. Beyond charges, excluded volume effects and topology contribute, as they influence the extent to which other water molecules participate in the formation of new hydrogen bonds.[48] We shall see that an effective quantity in capturing access of water molecules to form new hydrogen bonds to facilitate protein−water hydrogen bond dynamics is the average solvent-accessible surface area (SASA) relative to maximum values for a particular residue found in a large data set.[50]

We therefore compute the average SASA per residue during the simulation. The average SASA for residue i is $\langle \mathrm{SASA}_i \rangle$. We use GROMACS to compute the mean relative accessible surface area (RSA) per residue[50]

$$\mathrm{RSA}_i = \frac{\mathrm{SASA}_i}{\mathrm{SASA}_{i,\max}} \tag{2}$$

where $\mathrm{SASA}_{i,\max}$ is the maximum accessible surface area for residue i. We chose the empirical results of Tien et al.,[50] who obtained $\mathrm{SASA}_{i,\max}$ for a given residue from the largest value found among 3197 structures from the PDB, where chain-terminating residues were excluded, to obtain RSA values between 0 and 1. Below we present full results of hydrogen bond lifetimes, τ, vs RSA for all residues except those at the ends of the chains, as well as binned results as a guide to seeing trends in the data with RSA. For the binning, we used a sliding window averaging method along the RSA of each data type (anionic, cationic, polar, and nonpolar). A sliding window average has a window size (0.25) and step size of (0.125). The window moves to the right from left along RSA. The first length is 0.25 of RSA, then it moves by 0.125 every step until it reaches 1, i.e., the first window is 0 to 0.25, the next window is 0.125 to 0.25 + 0.125, and the last is 0.75 to 1.0.

We compute a retardation factor of the hydrogen bond lifetime, which results from the interaction between water and the protein, for a given region of RSA. This is motivated by the retardation factor computed for hydrogen bond lifetimes between water molecules near chemical groups of solutes.[48] To compute the retardation factor for protein−water hydrogen bonds in this work, the sliding window averages of each data type (anionic, cationic, polar, and nonpolar) were calculated with a sliding window length of 0.25 and an overlapping length of 0.16 along the RSA. Then, the retardation factors were computed as $\tau_{\mathrm{polar}}/\tau_{\mathrm{nonpolar}}$, $\tau_{\mathrm{cationic}}/\tau_{\mathrm{nonpolar}}$, and $\tau_{\mathrm{anionic}}/\tau_{\mathrm{nonpolar}}$ for polar, cationic, and anionic residues, respectively. The

https://doi.org/10.1021/acs.jpcb.3c03102
J. Phys. Chem. B 2023, 127, 7839−7847

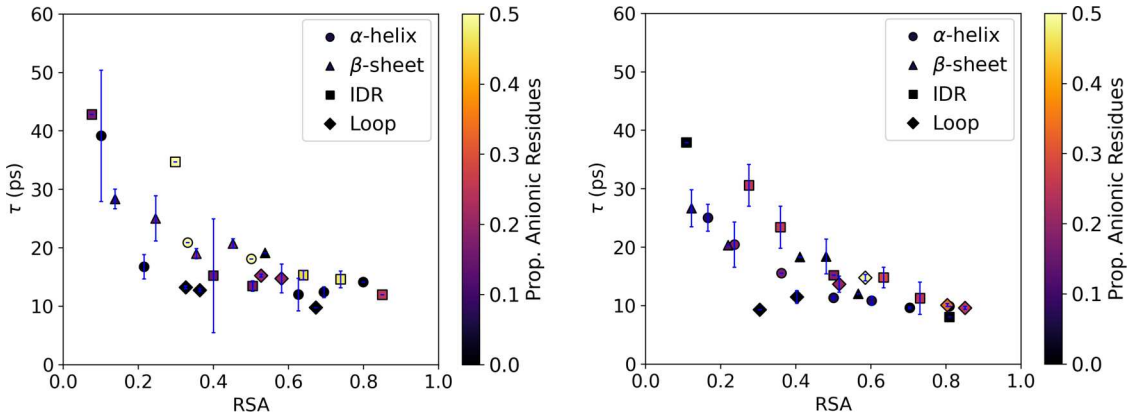

Figure 3. Hydrogen bond lifetime, τ, vs relative accessible surface area (RSA), defined by eq 2, for (left) SUMO-1 and (right) UBC9. The data presented was produced by a sliding window average along RSA for residues belonging to α-helices, β-sheets, IDRs, and loop regions. Error bars indicate one standard deviation. Coloring of each point corresponds to the proportion of anionic residues per window average. Note that the highest proportion of anionic residues is less than half the total number of residues.

retardation factors were plotted against the mean RSA value of each segment.

We shall see that for small RSA there is a large distribution of hydrogen bond lifetimes. When RSA is small, it is possible for a residue to be near the surface if the side chain is largely unexposed to the solvent or the residue may lie closer to the interior of the protein. These factors may determine if the hydrogen bond lifetime is large or small. We thus examine whether there is a correlation between the length of the hydrogen bond lifetime and the distance of the residue from the center of mass of the protein when RSA is small. For small RSA, we consider values below 0.3. We take a time of 30 ps as a cutoff, separating short and long hydrogen bond lifetimes, where times greater than 30 ps are considered long and the rest short. For all residues with long lifetimes ($\tau \geq 30$ ps) and with RSA below 0.3, we compute the distance of the center of mass of the residue from the center of mass of the protein. Similarly, for all residues with short lifetimes ($\tau < 30$ ps) and with RSA below 0.3, we compute the distance of the center of mass of the residue from the center of mass of the protein. We then examine if there is a correlation in the distance between the residue and center of mass of the protein and the average lifetime of hydrogen bonds between the residue and water molecules. We note that changing the cutoff to values somewhat below 30 ps or above 30 ps does not change the trends observed in the analysis.

3. RESULTS AND DISCUSSION

The lifetimes of protein−water hydrogen bonds for SUMO-1 and UBC9 are plotted in Figure 2 as a function of RSA. We separate lifetimes for hydrogen bonds between water and anionic, cationic, polar, and nonpolar residue side chains. Looking first at the overall trends in the data, we see that the lifetime for hydrogen bonds between water molecules and protein generally increases as RSA becomes smaller. For nonpolar residues, the variation in the lifetime with RSA is small until RSA becomes smaller than about 0.4, where the lifetime increases strikingly with smaller values of RSA. For polar and cationic residues, a similar trend is seen, though there is a more noticeable increase in the lifetime with decreasing RSA over the full range of RSA plotted than seen for nonpolar residues. For anionic residues, we see for UBC9 that the lifetimes steadily increase with smaller RSA values, while for SUMO-1 the variation of lifetime with RSA is small for RSA above 0.4 and increases significantly with smaller RSA below 0.4.

RSA quantifies the average exposure of a residue to water relative to its maximum SASA.[50] Because smaller RSA corresponds to less access to water molecules than large RSA, we expect smaller values of RSA to correspond to longer lifetimes. Hydrogen bonds can rearrange when water molecules are nearby to serve as new hydrogen bond donors or acceptors, but that is less likely when RSA is small. In the jump model developed by Laage and Hynes,[48,49,60] hydrogen bonds between water molecules rearrange as an acceptor moves toward a donor, forming a transition state whereby the hydrogen bond between two water molecules jumps to form a new hydrogen bond. Similarly, for a hydrogen bond between a water molecule and a protein residue, there needs to be another nearby hydrogen bond donor or acceptor for rearrangement to occur. The overall trends seen in Figure 2 are consistent with this picture.

For a given RSA, the longest lifetimes are found for water molecules in contact with anionic residues, followed by cationic, polar, and nonpolar residues. This is generally the order found for hydrogen bonds between water molecules near residues of this kind and has been explained by the jump model.[48] Water molecules hydrogen bonded to anionic residues cannot easily reform a hydrogen bond with another water molecule. When the oxygen atom of a nearby water molecule moves toward the water that hydrogen bonds to the anion, the latter bond is less susceptible to break due to the relatively strong binding enthalpy so that the transition state to another hydrogen bond does not easily form. While there are some restrictions to rearrangement for water molecules interacting with cations, the water molecule can still rotate around the axis of the bond between the oxygen atom and cation to form a new hydrogen bond and is thereby less restricted than when hydrogen bonded to an anion.

To investigate the effect, if any, of secondary structure on the dynamics of hydrogen bonds between protein and water, a moving window average was applied across RSA values with respect to the structure (Section 2). The results are plotted in Figure 3. Additionally, the proportion of anionic residues is indicated by the color, with lighter data points corresponding

https://doi.org/10.1021/acs.jpcb.3c03102
J. Phys. Chem. B 2023, 127, 7839−7847

to greater anionic character of the structural element to which the residue belongs.

Overall, lighter colors are seen to correspond to somewhat longer lifetimes for a given RSA, as is expected from the results seen in Figure 2. In many cases, the points with longer lifetimes correspond to IDRs, reflecting the tendency for disordered regions to contain charged residues, but in many other cases, longer lifetimes for a given RSA may correspond to structural elements, often β-strands and in some cases α-helices. Overall, there is no striking difference in values of the hydrogen bond lifetime between water molecules and residues of IDRs and lifetimes of water molecules hydrogen bonding to residues of structural elements of the proteins. Based on Figure 3, we see that the lifetime is dictated by RSA value, particularly for smaller values of RSA, and based on the results of Figures 2 and 3 also the charged nature of the residue, particularly noteworthy for anionic residues.

Returning to Figure 2, substantial variation in values of the lifetimes for a given RSA is observed for all residue classifications. The data plotted are listed in the Supporting Information in Tables S1 and S2, along with error estimates. We have carried out statistical analysis to identify any outliers in the data and to quantify if the differences in the average lifetimes of anionic, cationic, polar, and nonpolar residues in different regions of RSA are statistically significant. For the latter, we ran an ANOVA test[61] for the data in RSA intervals of 0−0.2, 0.2−0.4, 0.4−0.6, 0.6−0.8, and 0.8−1.0. The results of the ANOVA test are tabulated in the Supporting Information. The test confirms that differences in average lifetimes for anionic, cationic, polar, and nonpolar residues are statistically significant for all RSA except for the smallest values, in the range 0−0.2, for both SUMO-1 and UBC9. We will discuss the large variation in the lifetimes for small RSA below.

We also examined the data for any outliers from the first quartile, Q1; the third quartile, Q3; and the difference, IQR = Q3 − Q1. Data points that lie outside the range Q1 − 1.5 × IQR and Q3 + 1.5 × IQR are considered outliers.[62] This range in the data was computed for anionic, cationic, polar, and nonpolar residues of SUMO-1 and UBC9 again for RSA intervals 0−0.2, 0.2−0.4, 0.4−0.6, 0.6−0.8, and 0.8−1.0. The results are plotted in the Supporting Information as boxplots (Figure S7). From this analysis, only 11 residues out of 223 total for which hydrogen bond lifetimes are computed are outliers. They are indicated in the Supporting Information (Tables S1 and S2) and we discuss some of them now.

Consider first the data for SUMO-1, starting with RSA between 0.4 and 0.6. For RSA near 0.45, the residue with the longest lifetime is a polar residue, Ser61, with an average lifetime of 21.5 ps. Ser61 is identified as one of 11 outliers mentioned above. We find Ser61 to lie near several charged residues. On average, the minimum distance, i.e., the nearest distance between an atom of Ser61 and an atom of another residue, computed over the course of the MD simulation is 2.9 Å to Glu89. The average minimum distance to Arg63 is 3.4 Å. There are other residues with ionic groups for which the average minimum distance from Ser61 is small, specifically Lys48 (4.8 Å), Glu93 (6.6 Å), and Glu49 (6.7 Å). A snapshot indicating locations of these residues appears in Figure S1. We note that the long lifetime for Ser61, and other residues with exceptionally long lifetimes, may be affected by the limited length of the total simulation as conformers potentially not sampled could influence the density of nearby charged groups and thus the lifetime.

For RSA in the range 0.5 to 0.6, the residue with the longest hydrogen bond lifetime is a polar residue (Thr42), with a lifetime of 25.4 ps, and the residue with the shortest lifetime is GLY56, with a lifetime of 5.7 ps. The former is found in a loop and the latter in an IDR, so that neither lies in a structured region. As is evident in Figure 2, lifetimes for hydrogen bonds between water molecules and polar or nonpolar residues of 10 ps or less are not uncommon. It is noteworthy that the shortest one in the region we are considering involves an IDR, as we already concluded from Figure 3 that the structural features themselves are less important than the nature of the residue (anionic, nonpolar, etc.) and RSA. Here, we see two residues with nearly the same RSA and the same character (polar) exhibit very different lifetimes.

Like Ser61, the reason for the long lifetime of the hydrogen bond between water and the polar residue Thr42 of SUMO-1 is the proximity to several charged residues. The lifetime for Thr42, like Ser61, has been identified as one of 11 outliers. Water molecules in contact with ionic residues, particularly anionic, cannot easily rearrange to form new hydrogen-bonding partners with water molecules that hydrogen bond to Thr42, enhancing the lifetime of the hydrogen bond between water and Thr42. On average, the minimum distance between Thr42 and Asp73 is 3.5 Å, and Thr42 lies close to 3 lysine residues, an average minimum distance of 3.5 Å from Lys46, 5.5 Å from Lys37, and 5.9 Å from Lys39. A snapshot indicating the location of these residues appears in Figure S2. For Gly56, with a short lifetime of 5.7 ps, there are no charged residues within on average 8.3 Å. Even if there are some charged residues nearby, we expect that more sluggish dynamics occurs with a higher density of charged residues. For example, hydrogen bond dynamics between water and Gln69, with an RSA near 0.6, is also quite fast, but there is only one charged residue in the vicinity (Glu69 with an average minimum distance of 4.9 Å). At smaller RSA, but still above 0.2, the largest hydrogen bond lifetimes are all with either glutamic acid or aspartate. Some are found in IDRs and some in β-sheets. Again, we see that the structural element itself does not appear to be a major factor in the lifetime, but instead the ionic, particularly anionic, character of the residues.

Turning to UBC9, we see a similar pattern. Around RSA of 0.4, the hydrogen bond with the longest lifetime, 55.1 ps, is the polar contact Ser95, which is part of an IDR. While Ser95 is not identified as one of the 11 outliers, it nevertheless exhibits a long lifetime. Ser95 lies near many ionic residues including Glu98, with an average minimum distance of 2.3 Å; Asp102, with an average minimum distance of 2.0 Å; and Lys101, with an average minimum distance of 2.4 Å. Other nearby anionic residues include Asp100, Asp127, and Glu99, with average minimum distance of 5.6, 5.1, and 5.5 Å, respectively. A snapshot indicating the location of the residues appears in Figure S3. Other polar contacts in the range of RSA from 0.2 to 0.4 also exhibit the longest lifetimes near a particular RSA value. One is Asn124, with an average lifetime of 42.6 ps. Asp127 and Glu122 are found on average a minimum distance of 2.6 and 3.7 Å, respectively, from Asn124, shown in Figure S4. Ser71, with a somewhat shorter lifetime, also has two nearby anionic residues and two nearby cationic residues, all shown in Figure S5. Finally, Ile107, a nonpolar residue, has been identified as one of the 11 outliers. The lifetime, 31.4 ps, is exceptionally long for a nonpolar residue with an RSA of 0.33. Asp102 and Glu12 are found on average a minimum

https://doi.org/10.1021/acs.jpcb.3c03102
J. Phys. Chem. B 2023, 127, 7839−7847

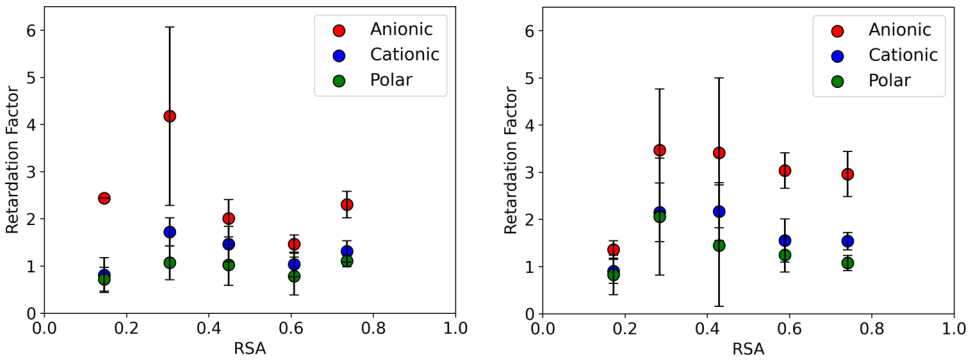

Figure 4. Retardation factor relative to lifetimes for nonpolar residues for (left) SUMO-1 and (right) UBC9 as a function of relative solvent-accessible surface area (RSA). Error bars indicate 1 standard deviation.

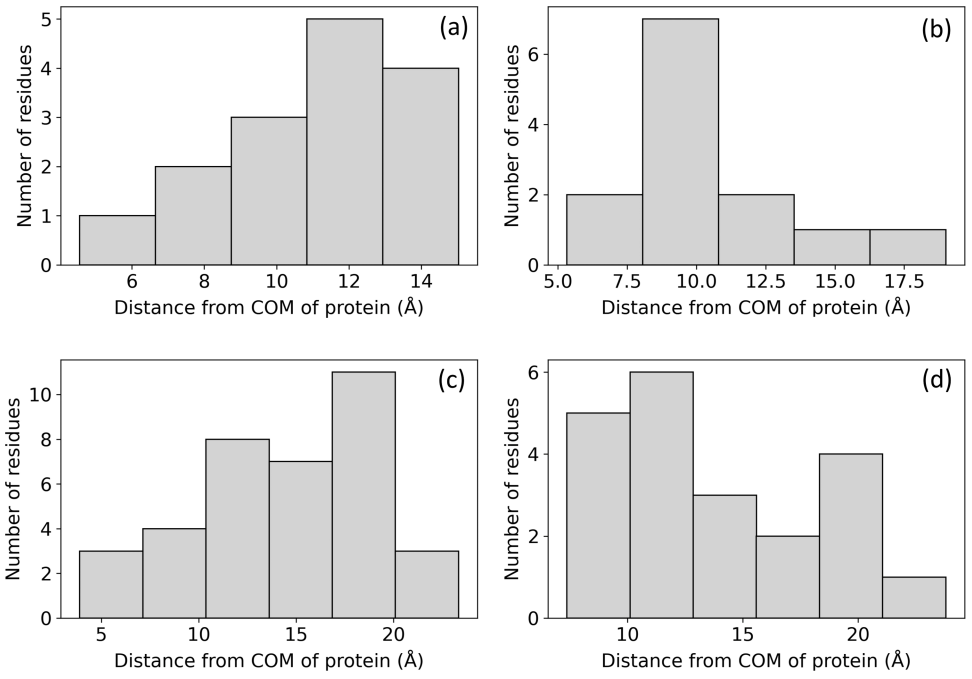

Figure 5. Distribution of distances between the center of mass of residues with small values of the relative solvent-accessible surface area (RSA) (less than 0.3) and the center of mass of the protein for (a) residues of SUMO-1 with $\tau < 30$ ps, (b) residues of SUMO-1 with $\tau \geq 30$ ps, (c) residues of UBC9 with $\tau < 30$ ps, and (d) residues of UBC9 with $\tau \geq 30$ ps. Histograms of SUMO-1 are plotted by dividing the length of x-axis in 5 equidistance windows. The total length represents the max−min of the distances. The bin sizes are 2.1 and 2.7 Å for (a, b), respectively. For UBC9, the data are divided into 6 equidistance windows. The bin sizes are 3.23 and 2.7 Å for (c, d), respectively.

distance of 3.4 and 4.8 Å, respectively. A snapshot indicating the location of nearby charged residues is shown in Figure S6.

For RSA below 0.2, there are no anionic residues and only a few cationic residues, as is also the case for SUMO-1. For both proteins, the lifetimes vary considerably when RSA is below 0.2, from a few ps to about 100 ps. As discussed further below, longer lifetimes are found where residues lie closer to the center of mass of the protein and shorter ones closer to the surface.

We find the lifetime of hydrogen bonds between water molecules and amino acids to depend on RSA, so we consider here an RSA-dependent retardation factor. Since lifetimes between water molecules and nonpolar residues are usually shortest for a given RSA, compared to hydrogen bonds between water and polar or charged residues, we define the retardation factor as the average lifetime for a polar, cationic, or anionic residue relative to the average lifetime for a nonpolar residue near a given RSA value. Specifically, the retardation factors are computed as $\tau_{polar}/\tau_{nonpolar}$, $\tau_{cationic}/\tau_{nonpolar}$, and $\tau_{anionic}/\tau_{nonpolar}$ for polar, cationic, and anionic residues, respectively.

In Figure 4, we plot the RSA-dependent retardation factor for SUMO-1 and UBC9. The lifetimes are averaged in intervals of 0.1 in RSA. We note that for the smallest RSA plotted, just below 0.2, the results of the ANOVA test indicate no statistical significance in the differences of the averages that are plotted, but for other RSA the differences are significant. The trends for both proteins are similar, though for the smaller SUMO-1 there is greater variation in the average value of the retardation factor around a given RSA compared to UBC9. For RSA larger than 0.4, average values of the retardation factor are between about 1 and 1.5 for polar residues, between about 1 and 2 for cationic residues, and between 1.5 and 3.5 for anionic residues.

For hydrogen bonds between solutes and water, the lifetime has been predicted to be affected by excluded volume, which affects the approach of water molecules that can serve as new

https://doi.org/10.1021/acs.jpcb.3c03102
J. Phys. Chem. B 2023, 127, 7839−7847

hydrogen bond acceptors or donors, and enthalpy of the hydrogen bond between the solute and water molecule, as this impacts the favorability of forming a new hydrogen bond with another water molecule.[48] These have been treated as separable effects.[48] As we have seen, high concentrations of charged groups lead to slower relaxation times. For UBC9, the charged groups are most highly concentrated for RSA between 0.3 and 0.5 (see Figure 2), and the average retardation factors are relatively large in this region. For SUMO-1, the density of charged groups is large near an RSA of 0.3 and again near 0.7 (Figure 2), which is consistent with somewhat higher average retardation factors for these RSA. We note that there may be other factors, such as the curvature of the surface of the protein, that we have not accounted for and that may also affect the dynamics of hydrogen bonds between water molecules and the proteins.[63−65]

For residues with small RSA values, there is a large distribution of lifetimes, τ, for hydrogen bonds between water molecules and residues, most of which have nonpolar side chains. We expect that the largest values of τ correspond to residues that tend to lie more in the interior of the protein and those with smaller values lie toward the surface. To illustrate this, we consider those residues with values of RSA below 0.3. We plot the distribution of distances between the center of mass of residues with large τ, chosen to be greater than 30 ps, and center of mass of the protein. We compare that with the distribution of distances between the center of mass of residues with small τ, taken to be less than 30 ps, and the center of mass of the protein. The results for SUMO-1 and UBC9 are plotted in Figure 5.

Consider first SUMO-1. As seen in Figure 5, the most probable distance of a residue with RSA less than 0.3 and $\tau <$ 30 ps is about 12 Å from the center of mass of SUMO-1, whereas it is about 9 Å for $\tau \geq 30$ ps. The mean distances are not so different due to the broad distribution of distances from the center of mass and are 11.2 Å for $\tau <$ 30 ps and 10.4 Å for $\tau \geq 30$ ps. Turning to UBC9, we see that the most probable distance of a residue with RSA less than 0.3 and $\tau <$ 30 ps is about 18 Å from the center of mass, whereas it is about 11 Å for $\tau \geq 30$ ps. Again, the mean distances are more similar than the most probable distances and are 14.5 Å for $\tau <$ 30 ps and 13.8 Å for $\tau \geq 30$ ps. Different choices of large and small cutoffs for τ change the distributions somewhat but the overall picture is consistent with long-lived hydrogen bonds found more in the interior of the protein and less accessible to water molecules that could participate in rearrangement of hydrogen bonds.

For larger RSA, above ≈0.2, we find statistically significant correlations between RSA and hydrogen bond lifetimes as well as differences in average lifetimes for residues with nonpolar, polar, cationic, and anionic side chains. However, for smaller RSA, a residue may be either near the surface with the side chain barely exposed or buried in the interior of the protein. These possibilities give rise to a large distribution of hydrogen bond lifetimes when RSA is small. We have seen upon further analysis (Figure 5) that the lifetimes correlate with the location of the residue when RSA is small, where longer lifetimes are typically associated with residues closer to the interior and shorter lifetimes with residues closer to the surface. Other approaches may more naturally distinguish whether the residue hydrogen bonding with water is closer to the surface or interior and may thereby yield a metric that correlates with hydrogen bond lifetime over its full range of values. The confinement index, which quantifies the number of protein atoms near a water molecule that could be taken to be hydrogen bonded to the protein, introduced by Persson, Söderhjelm, and Halle,[66] could serve as such a metric and will be investigated in future work.

4. CONCLUSIONS

We have examined the dynamics of hydrogen bonds between water molecules and two proteins, SUMO-1 and UBC9. The dynamics of water around IDPs has been reported to be more restricted than around structured proteins,[37−41] which has been attributed to the larger proportion of residues with charged groups. Both SUMO-1 and UBC9 contain structured regions as well as IDRs, and the influence of each on the dynamics of hydrogen bonds between protein and water was examined. The dynamics of the hydrogen bonds are largely affected by two factors, one the nature of the residue to which water hydrogen bonds, specifically if the side chain is anionic, cationic, polar, or nonpolar. The other is the time-averaged relative solvent-accessible surface area (RSA), which affects access of water molecules to form new hydrogen bonds. In addition to these two properties, the density of charged groups contributes to the lifetime of hydrogen bonds between water and residues that are either charged or neutral.

While the lifetimes of hydrogen bonds between protein and water are typically longest for those between water and anionic groups for a given RSA value, we have seen in some cases that they can be even longer for other kinds of interactions, such as water molecules interacting with residues with polar side chains. That can occur if there is a relatively high density of nearby charged residues, particularly anionic. In this case, there are fewer water molecules to serve as new hydrogen bond donors as their motion is hindered by relatively strong interactions with the anionic residues. This gives rise to apparent collective effects, whereby hydrogen bonds between water and polar or nonpolar residues are relatively long lived compared to the case when there are fewer nearby charged residues. This effect was observed in a previous study of water dynamics near IDPs and structured proteins of similar size,[42] where it was found that water dynamics near all groups, charged and neutral, of a protein appeared more restricted around IDPs, due to the relatively high density of charged groups. We note that a recent computational study of hydrogen bond rearrangement in water reveals collective reorientation dynamics during hydrogen bond rearrangement.[67] It would be of interest in future work to examine if similar collective dynamics of water occurs during hydrogen bond rearrangement at the surface of proteins. Studies of other members of the SUMO family (SUMO-2, SUMO-3, and SUMO-4), rich in both IDRs and structured regions, would also be useful to provide additional data for comparing hydrogen bond dynamics between protein and water near structured and disordered regions.

The results presented provide a picture of hydrogen bond dynamics at the surface of proteins with IDRs and structured regions for dilute systems. Liquid−liquid phase separation[46,47] associated with regions of high densities of IDPs and dilute IDPs could yield different kinds of hydrogen bond dynamics in different phases and a wider range of dynamics than those seen here.

https://doi.org/10.1021/acs.jpcb.3c03102
J. Phys. Chem. B 2023, 127, 7839−7847

■ ASSOCIATED CONTENT

Supporting Information

The Supporting Information is available free of charge at https://pubs.acs.org/doi/10.1021/acs.jpcb.3c03102.

Environment of SUMO-1 residues hydrogen bonding with water; environment of UBC9 residues hydrogen bonding with water; boxplots of τ and results of ANOVA test; τ vs RSA for SUMO-1; τ vs RSA for UBC9; link to $C(t)$ vs time, t, data for SUMO-1 and UBC9 on GitHub; and plots of τ vs simulation length (PDF)

■ AUTHOR INFORMATION

Corresponding Author

David M. Leitner − *Department of Chemistry, University of Nevada, Reno, Nevada 89557, United States;* orcid.org/0000-0002-3105-818X; Email: dml@unr.edu

Authors

Korey M. Reid − *Department of Chemistry, University of Nevada, Reno, Nevada 89557, United States; Department of Chemistry, Dartmouth College, Hanover, New Hampshire 03755, United States*

Humanath Poudel − *Department of Chemistry, University of Nevada, Reno, Nevada 89557, United States*

Complete contact information is available at: https://pubs.acs.org/10.1021/acs.jpcb.3c03102

Notes

The authors declare no competing financial interest.

■ ACKNOWLEDGMENTS

K.M.R. thanks Thomas Sisk for proof reading code and helpful insight on various and meaningful convergence metrics. Support from NSF grants CHE-1854271 and CHE-2245240 is gratefully acknowledged.

■ REFERENCES

(1) Tompa, P. Multisteric Regulation by Structural Disorder in Modular Signaling Proteins: An Extension of the Concept of Allostery. *Chem. Rev.* **2014**, *114*, 6715−6732.

(2) Theillet, F.-X.; Binolfi, A.; Frembgen-Kesner, T.; Hingorani, K.; Sarkar, M.; Kyne, C.; Li, C.; Crowley, P. B.; Gierasch, L.; Pielak, G. J.; et al. Physicochemical Properties of Cells and Their Effects on Intrinsically Disordered Proteins (IDPs). *Chem. Rev.* **2014**, *114*, 6661−6714.

(3) van der Lee, R.; Buljan, M.; Lang, B.; Weatheritt, R. J.; Daughdrill, G. W.; Dunker, A. K.; Fuxreiter, M.; Gough, J.; Gsponer, J.; Jones, D. T.; et al. Classification of Intrinsically Disordered Regions and Proteins. *Chem. Rev.* **2014**, *114*, 6589−6631.

(4) Salvay, A. G.; Grigera, J. R.; Colombo, M. F. The Role of Hydration on the Mechanism of Allosteric Regulation: In Situ Measurements of the Oxygen-Linked Kinetics of Water Binding to Hemoglobin. *Biophys. J.* **2003**, *84*, 564−570.

(5) Leitner, D. M.; Hyeon, C.; Reid, K. M. Water-Mediated Biomolecular Dynamics and Allostery. *J. Chem. Phys.* **2020**, *152*, No. 240901.

(6) Ebbinghaus, S.; Kim, S. J.; Heyden, M.; Yu, X.; Heugen, U.; Gruebele, M.; Leitner, D. M.; Havenith, M. An Extended Dynamical Hydration Shell around Proteins. *Proc. Natl. Acad. Sci. U.S.A.* **2007**, *104*, 20749−20752.

(7) Leitner, D. M.; Gruebele, M.; Havenith, M. Solvation Dynamics of Biomolecules: Modeling and Terahertz Experiments. *HFSP J.* **2008**, *2*, 314−323.

(8) Leitner, D. M.; Havenith, M.; Gruebele, M. Biomolecule Large Amplitude Motion and Solvation Dynamics: Modeling and Probes from Thz to X-Rays. *Int. Rev. Phys. Chem.* **2006**, *25*, 553−582.

(9) Heyden, M.; Tobias, D. J. Spatial Dependence of Protein-Water Collective Hydrogen Bond Dynamics. *Phys. Rev. Lett.* **2013**, *111*, No. 218101.

(10) Heyden, M. Heterogeneity of Water Structure and Dynamics at the Protein-Water Interface. *J. Chem. Phys.* **2019**, *150*, No. 094701.

(11) Charkhesht, A.; Regmi, C. K.; Mitchell-Koch, K. R.; Cheng, S.; Vinh, N. Q. High-Precision Megahertz-to-Terahertz Dielectric Spectroscopy of Protein Collective Motions and Hydration Dynamics. *J. Phys. Chem. B* **2018**, *122*, 6341−6350.

(12) Bellissent-Funel, M.-C.; Hassanali, A.; Havenith, M.; Henchman, R.; Pohl, P.; Sterpone, F.; van der Spoel, D.; Xu, Y.; Garcia, A. E. Water Determines the Structure and Dynamics of Proteins. *Chem. Rev.* **2016**, *116*, 7673−7697.

(13) Bagchi, B. Water Dynamics in the Hydration Layer around Proteins and Miscelles. *Chem. Rev.* **2005**, *105*, 3197−3219.

(14) Mondal, S.; Bagchi, B. From Structure and Dynamics to Biomolecular Functions: The Ubiquitous Role of Solvent in Biology. *Curr. Opin. Struct. Biol.* **2022**, *77*, No. 102462.

(15) Nandi, N.; Bagchi, B. Dielectric Relaxation of Biological Water. *J. Phys. Chem. B* **1997**, *101*, 10954−10961.

(16) Pal, S. K.; Peon, J.; Bagchi, B.; Zewail, A. H. Biological Water: Femtosecond Dynamics of Macromolecular Hydration. *J. Phys. Chem. B* **2002**, *106*, 12376−12395.

(17) Martin, D. R.; Matyushov, D. V. Terahertz Absorption of Lysozyme in Solution. *J. Chem. Phys.* **2017**, *147*, No. 084502.

(18) Fogarty, A. C.; Laage, D. Water Dynamics in Protein Hydration Shells: The Molecular Origins of the Dynamical Perturbation. *J. Phys. Chem. B* **2014**, *118*, 7715−7729.

(19) Gavrilov, Y.; Leuchter, J. D.; Levy, Y. On the Coupling between the Dynamics of Protein and Water. *Phys. Chem. Chem. Phys.* **2017**, *19*, 8243−8257.

(20) Doan, L. C.; Dahanayake, J. N.; Mitchell-Koch, K. R.; Singh, A. K.; Vinh, N. Q. Probing Adaptation of Hydration and Protein Dynamics to Temperature. *ACS Omega* **2022**, *7*, 22020−22031.

(21) Gnanasekaran, R.; Xu, Y.; Leitner, D. M. Dynamics of Water Clusters Confined in Proteins: A Molecular Dynamics Simulation Study of Interfacial Waters in a Dimeric Hemoglobin. *J. Phys. Chem. B* **2010**, *114*, 16989−16996.

(22) Xu, Y.; Leitner, D. M. Vibrational Energy Flow through the Green Fluorescent Protein-Water Interface: Communication Maps and Thermal Boundary Conductance. *J. Phys. Chem. B* **2014**, *118*, 7818−7826.

(23) Xu, Y.; Havenith, M. Perspective: Watching Low-Frequency Vibrations of Water in Biomolecules by Thz Spectroscopy. *J. Chem. Phys.* **2015**, *143*, No. 170901.

(24) Bertalan, É.; Lešnik, S.; Bren, U.; Bondar, A. N. Protein-Water Hydrogen-Bond Networks of G Protein-Coupled Receptors: Graph-Based Analyses of Static Structures and Molecular Dynamics. *J. Struct. Biol.* **2020**, *212*, No. 107634.

(25) Karathanou, K.; Lazaratos, M.; Bertalan, E.; Siemers, M.; Buzar, K.; Schertler, G. F. X.; del Val, C.; Bondar, A.-N. A Graph-Based Approach Identifies Dynamic H-Bond Communication Networks in Spike Protein S of Sars-Cov-2. *J. Struct. Biol.* **2020**, *212*, No. 107617.

(26) Bondar, A.-N. Graphs of Hydrogen-Bond Networks to Dissect Protein Conformational Dynamics. *J. Phys. Chem. B* **2022**, *126*, 3873−3894.

(27) Yu, X.; Park, J.; Leitner, D. M. Thermodynamics of Protein Hydration Computed by Molecular Dynamics and Normal Modes. *J. Phys. Chem. B* **2003**, *107*, 12820−12829.

(28) Pandey, H. D.; Leitner, D. M. Thermodynamics of Hydration Water around an Antifreeze Protein: A Molecular Simulation Study. *J. Phys. Chem. B* **2017**, *121*, 9498−9507.

(29) Xu, Y.; Gnanasekaran, R.; Leitner, D. M. Analysis of Hydrogen Bond Dynamics at the Surface of an Antifreeze Protein. *J. At., Mol., Opt. Phys.* **2012**, *2012*, 1−6.

(30) Chong, S.-H.; Ham, S. Anomalous Dynamics of Water Confined in Protein−Protein and Protein−DNA Interfaces. *J. Phys. Chem. Lett.* **2016**, *7*, 3967−3972.
(31) Reid, K. M.; Yu, X.; Leitner, D. M. Change in Vibrational Entropy with Change in Protein Volume Estimated with Mode Grüneisen Parameters. *J. Chem. Phys.* **2021**, *154*, No. 055012.
(32) Poudel, H.; Leitner, D. M. Energy Transport in Class B Gpcrs: Role of Protein-Water Dynamics and Activation. *J. Phys. Chem. B* **2022**, *126*, 8362−8373.
(33) Poudel, H.; Leitner, D. M. Locating Dynamic Contributions to Allostery Via Determining Rates of Vibrational Energy Transfer. *J. Chem. Phys.* **2023**, *158*, No. 015101.
(34) Reid, K. M.; Yamato, T.; Leitner, D. M. Variation of Energy Transfer Rates across Protein−Water Contacts with Equilibrium Structural Fluctuations of a Homodimeric Hemoglobin. *J. Phys. Chem. B* **2020**, *124*, 1148−1159.
(35) Leitner, D. M.; Pandey, H. D.; Reid, K. M. Energy Transport across Interfaces in Biomolecular Systems. *J. Phys. Chem. B* **2019**, *123*, 9507−9524.
(36) Päslack, C.; Schäfer, L. V.; Heyden, M. Protein Flexibility Reduces Solvent-Mediated Friction Barriers of Ligand Binding to a Hydrophobic Surface Patch. *Phys. Chem. Chem. Phys.* **2021**, *23*, 5665−5672.
(37) Rani, P.; Biswas, P. Local Structure and Dynamics of Hydration Water in Intrinsically Disordered Proteins. *J. Phys. Chem. B* **2015**, *119*, 10858−10867.
(38) Mukhopadhyay, S. The Dynamism of Intrinsically Disordered Proteins: Binding-Induced Folding, Amyloid Formation, and Phase Separation. *J. Phys. Chem. B* **2020**, *124*, 11541−11560.
(39) Chowdhury, A.; Kovalenko, S. A.; Aramburu, I. V.; Tan, P. S.; Ernsting, N. P.; Lemke, E. A. Mechanism-Dependent Modulation of Ultrafast Interfacial Water Dynamics in Intrinsically Disordered Protein Complexes. *Angew. Chem., Int. Ed.* **2019**, *58*, 4720−4724.
(40) Arya, S.; Singh, A. K.; Bhasne, K.; Dogra, P.; Datta, A.; Das, P.; Mukhopadhyay, S. Femtosecond Hydration Map of Intrinsically Disordered A-Synuclein. *Biophys. J.* **2018**, *114*, 2540−2551.
(41) Gallat, F.-X.; Laganowsky, A.; Wood, K.; Gabel, F.; Eijck, Lv.; Wuttke, J.; Moulin, M.; Härtlein, M.; Eisenberg, D.; Colletier, J.-P.; et al. Dynamical Coupling of Intrinsically Disordered Proteins and Their Hydration Water: Comparison with Folded Soluble and Membrane Proteins. *Biophys. J.* **2012**, *103*, 129−136.
(42) Reid, K. M.; Singh, A. K.; Bikash, C. R.; Wei, J.; Tal-Gan, Y.; Vinh, N. Q.; Leitner, D. M. The Origin and Impact of Bound Water around Intrinsically Disordered Proteins. *Biophys. J.* **2022**, *121*, 540−551.
(43) Salvi, N.; Abyzov, A.; Blackledge, M. Solvent-Dependent Segmental Dynamics in Intrinsically Disordered Proteins. *Sci. Adv.* **2019**, *5*, No. eaax2348.
(44) Sampson, D. A.; Wang, M.; Matunis, M. J. The Small Ubiquitin-Like Modifier-1 (SUMO-1) Consensus Sequence Mediates UBC9 Binding and Is Essential for SUMO-1 Modification. *J. Biol. Chem.* **2001**, *276*, 21664−21669.
(45) Cheng, X. Protein Sumoylation and Phase Separation: Partners in Stress? *Trends Biochem. Sci.* **2023**, *48*, 417−419.
(46) McCarty, J.; Delaney, K. T.; Danielsen, S. P. O.; Fredrickson, G. H.; Shea, J.-E. Complete Phase Diagram for Liquid-Liquid Phase Separation of Intrinsically Disordered Proteins. *J. Phys. Chem. Lett.* **2019**, *10*, 1644−1652.
(47) Pezzotti, S.; König, B.; Ramos, S.; Schwaab, G.; Havenith, M. Liquid-Liquid Phase Separation? Ask the Water! *J. Phys. Chem. Lett.* **2023**, *14*, 1556−1563.
(48) Laage, D.; Elsaesser, T.; Hynes, J. T. Water Dynamics in the Hydration Shells of Biomolecules. *Chem. Rev.* **2017**, *117*, 10694−10725.
(49) Laage, D.; Stirnemann, G.; Sterpone, F.; Rey, R.; Hynes, J. T. Reorientation and Allied Dynamics in Water and Aqueous Solutions. *Annu. Rev. Phys. Chem.* **2011**, *62*, 395−416.
(50) Tien, M. Z.; Meyer, A. G.; Sydykova, D. K.; Spielman, S. J.; Wilke, C. O. Maximum Allowed Solvent Accessibilites of Residues in Proteins. *PLoS One* **2013**, *8*, No. e80635.
(51) Brooks, B. R.; Brooks, C. L.; Mackerell, A. D.; Nilsson, L.; Petrella, R. J.; Roux, B.; Won, Y.; Archontis, G.; Bartels, C.; Boresch, S.; et al. CHARMM: The Biomolecular Simulation Program. *J. Comput. Chem.* **2009**, *30*, 1545−1614.
(52) Huang, J.; Rauscher, S.; Nawrocki, G.; Ran, T.; Feig, M.; de Groot, B. L.; Grubmuller, H.; MacKerell, A. D. CHARMM36m: An Improved Force Field for Folded and Intrinsically Disordered Proteins. *Nat. Methods* **2017**, *14*, 71−73.
(53) van der Spoel, D.; Lindahl, E.; Hess, B.; Groenhof, G.; Mark, A. E.; Berendsen, H. J. C. Gromacs: Fast, Flexible, and Free. *J. Comput. Chem.* **2005**, *26*, 1701−1718.
(54) Abraham, M. J.; Murtola, T.; Schulz, R.; Páll, S.; Smith, J. C.; Hess, B.; Lindahl, E. Gromacs: High Performance Molecular Simulations through Multi-Level Parallelism from Laptops to Supercomputers. *SoftwareX* **2015**, *1−2*, 19−25.
(55) Bernstein, F. C.; Koetzle, T. F.; Williams, G. J. B.; Meyer, E. F.; Brice, M. D.; Rodgers, J. R.; Kennard, O.; Shimanouchi, T.; M, T. The Protein Data Bank. A Computer-Based Archival File for Macromolecular Structures. *Eur. J. Biochem.* **1977**, *80*, 319−324.
(56) Jorgensen, W. L.; Chandrasekhar, J.; Madura, J. D.; Impey, R. W.; Klein, M. L. Comparison of Simple Potential Functions for Simulating Liquid Water. *J. Chem. Phys.* **1983**, *79*, 926−935.
(57) Darden, T.; York, D.; Peterson, L. Particle Mesh Ewald: An N Log(N) Method for Ewald Sums in Large Systems. *J. Chem. Phys.* **1993**, *98*, 10089−10092.
(58) Grubmüller, H.; Heller, H.; Windemuth, A.; Schulten, K. Generalized Verlet Algorithm for Efficient Molecular Dynamics Simulations with Long-Range Interactions. *Mol. Simul.* **1991**, *6*, 121−142.
(59) Bussi, G.; Donadio, D.; Parrinello, M. Canonical Sampling through Velocity Rescaling. *J. Chem. Phys.* **2007**, *126*, No. 014101.
(60) Laage, D.; Hynes, J. T. A Molecular Jump Mechanism of Water Reorientation. *Science* **2006**, *311*, 832−835.
(61) Virtanen, P.; Gommers, R.; Oliphant, T. E.; Haberland, M.; Reddy, T.; Cournapeau, D.; Burovski, E.; Peterson, P.; Weckesser, W.; Bright, J.; et al. Scipy 1.0: Fundamental Algorithms for Scientific Computing in Python. *Nat. Methods* **2020**, *17*, 261−272.
(62) Dekking, F. M.; Kraaikamp, C.; Lopuhaä, H. P.; Meester, L. E. *A Modern Introduction to Probability and Statistics: Understanding Why and How*; Springer: London, 2005.
(63) Dahanayake, J. N.; Mitchell-Koch, K. R. Entropy Connects Water Structure and Dynamics in Protein Hydration Layer. *Phys. Chem. Chem. Phys.* **2018**, *20*, 14765−14777.
(64) Dahanayake, J. N.; Shahryari, E.; Roberts, K. M.; Heikes, M. E.; Kasireddy, C.; Mitchell-Koch, K. R. Protein Solvent Shell Structure Provides Rapid Analysis of Hydration Dynamics. *J. Chem. Inf. Model.* **2019**, *59*, 2407−2422.
(65) Heyden, M.; Havenith, M. Combining THz Spectroscopy and MD Simulations to Study Protein-Hydration Coupling. *Methods* **2010**, *52*, 74−83.
(66) Persson, F.; Söderhjelm, P.; Halle, B. How Proteins Modify Water Dynamics. *J. Chem. Phys.* **2018**, *148*, No. 215103.
(67) Offei-Danso, A.; Morzan, U. N.; Rodriguez, A.; Hassanali, A.; Jelic, A. The Collective Burst Mechanism of Angular Jumps in Liquid Water. *Nat. Comm.* **2023**, *14*, No. 1345.

https://doi.org/10.1021/acs.jpcb.3c03102
J. Phys. Chem. B 2023, 127, 7839−7847